

## On an isotropic porous solid cylinder: the analytical solution and sensitivity analysis of the pressure\*

H. ASGHARI<sup>1</sup>, L. MILLER<sup>2</sup>, R. PENTA<sup>2,†</sup>, J. MERODIO<sup>1</sup>

1. Departamento de Matemática Aplicada a las TIC, ETS de Ingeniería de Sistemas Informáticos, Universidad Politécnica de Madrid, Madrid 28031, Spain;
2. School of Mathematics and Statistics, University of Glasgow, Glasgow G12 8QQ, U. K.

(Received May 8, 2024 / Revised Jul. 10, 2024)

**Abstract** Within this work, we perform a sensitivity analysis to determine the influence of the material input parameters on the pressure in an isotropic porous solid cylinder. We provide a step-by-step guide to obtain the analytical solution for a porous isotropic elastic cylinder in terms of the pressure, stresses, and elastic displacement. We obtain the solution by performing a Laplace transform on the governing equations, which are those of Biot's poroelasticity in cylindrical polar coordinates. We enforce radial boundary conditions and obtain the solution in the Laplace transformed domain before reverting back to the time domain. The sensitivity analysis is then carried out, considering only the derived pressure solution. This analysis finds that the time  $t$ , Biot's modulus  $M$ , and Poisson's ratio  $\nu$  have the highest influence on the pressure whereas the initial value of pressure  $P_0$  plays a very little role.

**Key words** sensitivity analysis, Laplace transform, cylindrical polar coordinate, Biot's modulus, cylinder

**Chinese Library Classification** O343

**2010 Mathematics Subject Classification** 76S05, 74A99, 35Q62

### 1 Introduction

The theory of poroelasticity describes the effective mechanical behavior of a porous elastic material with fluid filled pores. The theory was first developed in Refs. [1]–[4] from experimental observations. In physical scenarios where the interactions between the deformable solid and the fluid take place on the porescale, the theory is applicable to capture the behavior. The approach has been applied to many scenarios including modeling of hard hierarchical tissues such as bones<sup>[5–6]</sup>. It is also applicable to soft biological tissues including the heart (myocardium) and artery walls<sup>[7–10]</sup> as well as the interstitial matrix of biological tissues which can either be healthy or tumorous<sup>[11–12]</sup>. Applications of the theory also exist beyond animal biology, such

---

\* Citation: ASGHARI, H., MILLER, L., PENTA, R., and MERODIO, J. On an isotropic porous solid cylinder: the analytical solution and sensitivity analysis of the pressure. *Applied Mathematics and Mechanics (English Edition)*, **45**(9), 1499–1522 (2024) <https://doi.org/10.1007/s10483-024-3144-7>

† Corresponding author, E-mail: Raimondo.Penta@glasgow.ac.uk

Project supported by the Engineering and Physical Sciences Research Council of U. K. (Nos. EP/S030875/1, EP/T017899/1, and EP/T517896/1)

©The Author(s) 2024

as in artificial constructs that are used for regenerative therapies, biomimetic materials<sup>[13–14]</sup>, soil, and porous rocks<sup>[15–16]</sup>.

Solutions to boundary value problems involving partial differential equations equipped with appropriate boundary and initial conditions are well sought when addressing real-world problems. In some cases it is possible to determine a solution only numerically; however, there are a variety of scenarios where analytical solutions can be found. The solutions to the governing equations of porous media have been presented for a variety of geometries and techniques in the literature. Analytical solutions for porous cylinders, spheres, and boreholes are presented in Ref. [17], with the cylinder problem first investigated in Ref. [18]. The solutions provide expressions for pressure, stresses, and elastic displacement. Numerically there has also been a variety of approaches taken to determine the solution, and a review of these techniques can be found in Ref. [19].

The solutions that can be found involve a variety of parameters. Each of these parameters will have a different significance on the overall pressure, stress, or displacement. The importance of each parameter can be determined via a sensitivity analysis. Additionally, the sensitivity analysis leads to the understanding of how the interactions between the different input parameters affect the solution output.

The sensitivity analysis is implemented to examine the impact of the different input values on the model behavior, and it can have a significant role in different areas of model development such as model substantiation, research prioritization, model improvement, and model verification<sup>[20]</sup>. Moreover, the sensitivity analysis gives a comprehensive overview of how the interactions between the different input parameters affect the behavior of the model<sup>[22]</sup>. Recently, various areas of engineering and science that investigate complex models with industrial applications to biomechanics have utilized the sensitivity analysis technique<sup>[23–24]</sup>. This led to the application of sensitivity analysis to study the inflation of tubular structures in Ref. [25] and closely related problems<sup>[23–24,26–28]</sup>. Obtaining a thorough understanding of the mechanical behavior of a material is important, as it requires quantifying and qualifying the degree of significance of the input parameters and their contributions to the output of the model. The sensitivity analysis addresses these points, and in particular, it evaluates the behavior of a model focusing on how the input parameters interact with the output variables.

There has been a categorization for sensitivity analysis methods. One of the most prominent is proposed by Frey and Patil<sup>[29]</sup>. They segmented the sensitivity analysis methods into three groups: (i) the mathematical approach that encompasses the automatic differentiation, the nominal range, log-odds ratio, and the break-even analysis; (ii) the graphical approach that entails the visualization tools such as scatter plots and heat maps; (iii) the statistical approach that includes probabilistic models with simulation methods and the corresponding estimators. The Sobol method, the Fourier amplitude sensitivity test (FAST) method, the regression analysis, and the Morris method are defined in the framework of the statistical sensitivity analysis methods. Some of these methods are applied under some constraints; for example the Morris and regression methods can be applied to monotonic models, while the Sobol and FAST methods can be implemented in complex problems with non-monotonic and non-linear behavior. Recent works<sup>[25,30]</sup> applied the Sobol and the FAST methods to study the extension, inflation, and torsion of a circular cylindrical tube in the presence of residual stresses.

Within this work, we first find an analytic solution to the equations that describe the mechanical behavior of a porous material using techniques described in Refs. [17]–[18]. We investigate a solid cylinder whose microstructure consists of a porous elastic matrix. The elastic matrix of the solid cylinder is assumed to be isotropic. We begin by introducing the governing equations of the porous media in cylindrical polar coordinates. We then perform a Laplace transformation on the equations and impose radial stress boundary conditions in order to find the solution in the Laplace transformed domain. We require our solution to be in the time domain, and to achieve this, we perform an inverse Laplace transformation. This allows us to

obtain an analytical solution for the governing equations of porous media. To better understand our results and the behavior of a porous elastic cylinder, we investigate the pressure solution via a sensitivity analysis. This allows us to determine which of the input parameters has the greatest influence on the pressure in a porous elastic isotropic cylinder. This can be useful for informing the design of biomimetic materials, as we can determine which material parameter (input) provides the greatest change in the material response (output).

The isotropic porous cylinder considered in this work could well describe hard hierarchical tissues, such as bones. A porous media approach to modeling bones has previously been studied<sup>[5,31–32]</sup>. The bone can be described as a porous solid, where the pores are filled with bone marrow, blood, or interstitial fluid and cells<sup>[32–33]</sup>. Bones remodel due to stress, injury or growth via a process regulated by mechanosensitive cells called osteocyte which can be found in the interstitial fluid of the pores<sup>[32,34]</sup>.

We note that a key feature of bone remodeling is the interstitial pressure as summarized in Ref. [35]. Solelmani et al.<sup>[35]</sup> stated that recent studies have provided evidence that the pressure and velocity of the interstitial fluid flowing through the pores of bones play a significant role in the bone remodeling process<sup>[36–37]</sup>. Ghiasi et al.<sup>[36]</sup> also stated that the interstitial fluid velocity and the shear stress within the bones, which the interstitial velocity creates, may influence the cells responsible for bone healing. For this reason, we investigate the pressure in an isotropic porous cylinder via a sensitivity analysis with a future application to bone remodeling in mind.

The paper is organized as follows. In Section 2, we find the solution analytically to the equations governing a porous elastic cylinder. We first introduce the governing equations for porous media in cylindrical polar coordinates. In Subsection 2.1, we perform a Laplace transform on the equations and impose radial stress boundary conditions in order to find the solution in the Laplace transformed domain. In Subsection 2.2, we wish to revert our solution back to the time domain so we need to perform an inverse Laplace transformation. In Subsection 2.3, we expand and simplify the solution obtained for the pressure to carry out the sensitivity analysis. In Section 3, we provide an in-depth overview of the sensitivity analysis technique and explain the methods that we use to investigate the parameters influencing the pressure in a porous elastic isotropic cylinder. In Section 4, we apply the Sobol method to the expanded and simplified pressure expression to investigate the role that each of the parameters has on the resulting pressure. Finally, in Section 5, we contextualize the solution at hand and provide concluding remarks as well as future perspectives for this work.

## 2 Problem formulation

In this section, we derive the analytical solution to the equations governing an isotropic porous elastic cylinder. The analytical solution has been considered in Refs. [17]–[18], yet here we present a re-derivation with full steps included to specifically aim at giving a first insight on the topic and solution method to students and scientists who are not familiar with the subject. We note that the steps carried out here are of the same type even if we were to choose a material that is not isotropic, i.e., with different symmetries. We have the solid porous elastic cylinder which we wish to consider under the radial inflation (see Fig. 1). To begin, we can write the displacement field in cylindrical polar coordinates for the cylinder as

$$\mathbf{u} = u_r \mathbf{e}_r + u_\theta \mathbf{e}_\theta + u_z \mathbf{e}_z. \tag{1}$$

We consider an axisymmetric model, plane strain, so that the displacement field  $\mathbf{u}$  reduces to

$$\mathbf{u} = u_r \mathbf{e}_r + 0 \mathbf{e}_\theta + 0 \mathbf{e}_z = (u(r), 0, 0) \quad \text{for radial inflation.} \tag{2}$$

There is only one equilibrium equation, which (with axial symmetry) can be written as

$$\frac{\partial \sigma_{rr}}{\partial r} + \frac{\sigma_{rr} - \sigma_{\theta\theta}}{r} = 0, \tag{3}$$

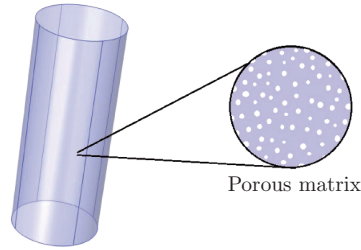


**Fig. 1** The cylinder and its zooming in the pore microstructure (color online)

in terms of the (cylindrical) components of the stress tensor  $\boldsymbol{\sigma}$ . The stress of the material can be written as

$$\boldsymbol{\sigma} = \lambda \text{tr}(\mathbf{e})\mathbf{I} + 2\mu\mathbf{e} - \alpha M\zeta\mathbf{I}, \quad (4)$$

where we have the strain given by

$$\mathbf{e}(\mathbf{u}) = \frac{\nabla\mathbf{u} + (\nabla\mathbf{u})^T}{2}, \quad (5)$$

$\lambda$  is the Lamé constant, which can be written in terms of shear  $\mu$  and Poisson's ratio  $\nu$  as

$$\lambda = \frac{2\mu\nu}{1-2\nu}, \quad (6)$$

$\alpha$  is Biot's coefficient,  $M$  is Biot's modulus, and  $\zeta$  is the fluid content. It follows easily that one can write the stress-strain relations as

$$\sigma_{rr} = \frac{2\mu\nu}{1-2\nu}e + 2\mu e_{rr} - \alpha M\zeta, \quad (7)$$

$$\sigma_{\theta\theta} = \frac{2\mu\nu}{1-2\nu}e + 2\mu e_{\theta\theta} - \alpha M\zeta, \quad (8)$$

$$\sigma_{zz} = \frac{2\mu\nu}{1-2\nu}e - \alpha M\zeta, \quad (9)$$

and similarly the pressure yields

$$p = M(\zeta - \alpha e), \quad (10)$$

where  $e = e_{rr} + e_{\theta\theta}$ . Then,  $e_{rr}$ ,  $e_{\theta\theta}$ , and the trace of the strain tensor  $\mathbf{e}$  can be written as

$$e_{rr} = \frac{\partial u_r}{\partial r}, \quad (11)$$

$$e_{\theta\theta} = \frac{u_r}{r}, \quad (12)$$

$$\text{tr}(\mathbf{e}) = e = \frac{\partial u_r}{\partial r} + \frac{u_r}{r} = \frac{1}{r} \frac{\partial(ru_r)}{\partial r}. \quad (13)$$

We can use the stresses (7)–(9) with the expressions (11)–(13) in the equilibrium (3) to obtain the Navier equation as

$$\frac{2\mu(1-\nu)}{(1-2\nu)} \left( \frac{\partial^2 u_r}{\partial r^2} + \frac{1}{r} \frac{\partial u_r}{\partial r} - \frac{u_r}{r^2} \right) - \alpha M \frac{\partial \zeta}{\partial r} = 0, \quad (14)$$

which can be rewritten as

$$\frac{\partial e}{\partial r} = \frac{\partial}{\partial r} \left( \frac{1}{r} \frac{\partial(ru_r)}{\partial r} \right) = \frac{\eta M}{\mu} \frac{\partial \zeta}{\partial r}, \quad (15)$$

where  $\eta = \frac{(1-2\nu)\alpha}{2(1-\nu)}$ . We can then integrate this equation once to yield

$$e = \frac{1}{r} \frac{\partial(ru_r)}{\partial r} = \frac{\eta M}{\mu} \zeta + 2B_1(t), \quad (16)$$

where  $B_1(t)$  is a constant function of the integration. This expression can be rearranged as

$$\frac{\partial(ru_r)}{\partial r} = \frac{r\eta M}{\mu}\zeta + 2B_1(t)r, \tag{17}$$

and integrating again gives

$$ru_r = \frac{\eta M}{\mu} \int r\zeta(r, t)dr + B_1(t)r^2 + B_2(t), \tag{18}$$

which, since  $B_2(t)$  is a constant function of integration, can be arranged as

$$u_r = \frac{\eta M}{r\mu} \int r\zeta(r, t)dr + B_1(t)r + \frac{B_2(t)}{r}. \tag{19}$$

Now using this latter expression for  $u_r$  and Eqs. (11)–(13), one can write

$$e_{rr} = \frac{\partial u_r}{\partial r} = \frac{-\eta M}{r^2\mu} \int r\zeta(r, t)dr + \frac{\eta M\zeta}{\mu} + B_1(t) - \frac{B_2(t)}{r^2}, \tag{20}$$

$$e_{\theta\theta} = \frac{u_r}{r} = \frac{\eta M}{r^2\mu} \int r\zeta(r, t)dr + B_1(t) + \frac{B_2(t)}{r^2}, \tag{21}$$

$$e = \frac{\partial u_r}{\partial r} + \frac{u_r}{r} = \frac{\eta M}{\mu}\zeta + 2B_1(t). \tag{22}$$

We can then use these latter expressions and (7)–(10) to obtain the stresses and the pressure, which are after some basic manipulations,

$$\sigma_{rr} = -\frac{2\eta M}{r^2} \int r\zeta(r, t)dr + \frac{2\mu}{1-2\nu}B_1(t) - \frac{2\mu}{r^2}B_2(t), \tag{23}$$

$$\sigma_{\theta\theta} = -\frac{2\eta M}{r^2} \int r\zeta(r, t)dr - 2\eta M\zeta + \frac{2\mu}{1-2\nu}B_1(t) + \frac{2\mu}{r^2}B_2(t), \tag{24}$$

$$\sigma_{zz} = -2\eta M\zeta + \frac{4\mu\nu}{1-2\nu}B_1(t), \tag{25}$$

$$p = M\zeta\left(1 - \frac{\alpha\eta M}{\mu}\right) - 2\alpha MB_1(t). \tag{26}$$

### 2.1 Radial stress boundary conditions

The inner surface of the cylinder is subjected to a uniform radial stress,  $\sigma_{rr} = -P_0$ , and the pore pressure is drained,  $p = 0$ , i.e., the boundary conditions are

$$\sigma_{rr} = -P_0, \quad p = 0 \quad \text{at} \quad r = r_0. \tag{27}$$

We begin with the diffusion equation in the axisymmetric case,

$$\frac{\partial\zeta}{\partial t} - c\frac{1}{r}\frac{\partial}{\partial r}\left(r\frac{\partial\zeta}{\partial r}\right) = 0, \tag{28}$$

where  $c$  is the consolidation coefficient. Then, by performing a Laplace transformation on the diffusion equation (28), we have

$$\frac{d^2\bar{\zeta}}{dr^2} + \frac{1}{r}\frac{d\bar{\zeta}}{dr} - \frac{s}{c}\bar{\zeta} = 0. \tag{29}$$

Solving this equation, we can find  $\bar{\zeta}$ , which is the Laplace transformed fluid content  $\zeta$  that forms part of the complete solution to the stresses and the pressures in Eqs. (23)–(26). Therefore, Eq. (29) has the general solution

$$\bar{\zeta} = D_1 I_0\left(r\sqrt{\frac{s}{c}}\right), \tag{30}$$

where  $I_0$  is the modified Bessel function of the first kind of order 0, and  $D_1$  is a constant function of  $s$  to be determined, with  $s$  being the transformation variable. We should note that

in Eq. (30) we have omitted a term containing  $K_0$ , the modified Bessel function of the second kind of order 0, for the solution of the problem at hand to be bounded when  $r = 0$ .

We can write down the Laplace transformation of the stress  $\sigma_{rr}$  (see Eq. (23)) as

$$\bar{\sigma}_{rr} = -\frac{2\eta M}{r^2} \int r \bar{\zeta}(r, s) dr + \frac{2\mu}{1-2\nu} \bar{B}_1(s). \quad (31)$$

We now substitute the general solution (30) into the Laplace transformed  $\bar{\sigma}_{rr}$  to obtain

$$\bar{\sigma}_{rr} = -\frac{2\eta M}{r^2} \int_0^r r' \left( D_1 I_0 \left( r' \sqrt{\frac{s}{c}} \right) \right) dr' + \frac{2\mu}{1-2\nu} \bar{B}_1(s), \quad (32)$$

where we note that for the solution to be bounded at  $r = 0$ , we have dropped the term associated with  $B_2(t)$ . Now we can perform the integration, for which we let  $x = r' \sqrt{\frac{s}{c}}$ ,  $\frac{dx}{dr'} = \sqrt{\frac{s}{c}}$ , and therefore  $dr' = \sqrt{\frac{c}{s}} dx$ . Under these circumstances we can write the integral in (32) as

$$\begin{aligned} \int_0^r r' \left( D_1 I_0 \left( r' \sqrt{\frac{s}{c}} \right) \right) dr' &= D_1 \int_0^{r\sqrt{\frac{s}{c}}} \left( x \sqrt{\frac{c}{s}} I_0(x) \sqrt{\frac{c}{s}} \right) dx \\ &= D_1 \frac{c}{s} (x I_1(x))_0^{r\sqrt{\frac{s}{c}}} = D_1 \sqrt{\frac{c}{s}} r I_1 \left( r \sqrt{\frac{s}{c}} \right). \end{aligned} \quad (33)$$

Using this latter expression and Eq. (31), one can write  $\bar{\sigma}_{rr}$  as

$$\bar{\sigma}_{rr} = -\frac{2\eta M}{r^2} \left( r \sqrt{\frac{c}{s}} D_1 I_1 \left( r \sqrt{\frac{s}{c}} \right) \right) + \frac{2\mu}{1-2\nu} \bar{B}_1(s). \quad (34)$$

We now move our attention to apply the Laplace transformation to the equation for the pressure (see Eq. (26)), which gives

$$p = M \bar{\zeta} \left( 1 - \frac{\alpha \eta M}{\mu} \right) - 2\alpha M \bar{B}_1(t). \quad (35)$$

Using the general solution (30) and the Laplace transformed  $\bar{p}$ , one obtains

$$\bar{p} = M \left( 1 - \frac{\alpha \eta M}{\mu} \right) D_1 I_0 \left( r \sqrt{\frac{s}{c}} \right) - 2\alpha M \bar{B}_1(s). \quad (36)$$

Using the boundary conditions (27) in Eqs. (34) and (36), we can solve for the unknowns  $\bar{B}_1$  and  $D_1$ . This gives

$$-P_0 = -\frac{2\eta M}{r_0^2} \left( r_0 \sqrt{\frac{c}{s}} D_1 I_1 \left( r_0 \sqrt{\frac{s}{c}} \right) \right) + \frac{2\mu}{1-2\nu} \bar{B}_1(s), \quad (37)$$

$$0 = M \left( 1 - \frac{\alpha \eta M}{\mu} \right) D_1 I_0 \left( r_0 \sqrt{\frac{s}{c}} \right) - 2\alpha M \bar{B}_1(s). \quad (38)$$

Now, one can eliminate  $\bar{B}_1$  from Eqs. (37) and (38) (use  $\frac{\mu}{1-2\nu} \times \text{Eq. (38)} + \alpha \times \text{Eq. (37)}$ ) to obtain

$$D_1 = \frac{-2\alpha P_0 r_0 \sqrt{s} (1-2\nu)(1-\nu)}{I_0(r_0 \sqrt{\frac{s}{c}}) (2\sqrt{s} r_0 (1-\nu)\mu - \alpha^2 M (1-2\nu) r_0 \sqrt{s}) - 2\alpha^2 M (1-2\nu)^2 \sqrt{c} I_1(r_0 \sqrt{\frac{s}{c}})}. \quad (39)$$

Then, using Eqs. (39) and (38), we obtain

$$\begin{aligned} \bar{B}_1 &= \frac{-2\alpha P_0 r_0 \sqrt{s} (1-2\nu)(1-\nu) (2\mu(1-\nu) - \alpha^2 M (1-2\nu)) I_0(r_0 \sqrt{\frac{s}{c}})}{4\mu\alpha(1-\nu) (I_0(r_0 \sqrt{\frac{s}{c}}) (2\sqrt{s} r_0 (1-\nu)\mu - \alpha^2 M (1-2\nu) r_0 \sqrt{s}) - 2\alpha^2 M (1-2\nu)^2 \sqrt{c} I_1(r_0 \sqrt{\frac{s}{c}}))} \\ &= \frac{2\mu(1-\nu) - \alpha^2 M (1-2\nu)}{4\mu\alpha(1-\nu)} I_0 \left( r_0 \sqrt{\frac{s}{c}} \right) D_1. \end{aligned} \quad (40)$$

Furthermore, using  $\bar{B}_1$  in the Laplace transformed  $\bar{\sigma}_{rr}$  (see Eq. (34)) and  $\bar{p}$  (see Eq. (36)), respectively, we obtain

$$\bar{\sigma}_{rr} = -\frac{2\eta M}{r} \sqrt{\frac{c}{s}} D_1 I_1\left(r\sqrt{\frac{s}{c}}\right) + \frac{2\mu(1-\nu) - \alpha^2 M(1-2\nu)}{2\alpha(1-\nu)(1-2\nu)} D_1 I_0\left(r_0\sqrt{\frac{s}{c}}\right), \tag{41}$$

and

$$\bar{p} = M\left(1 - \frac{\alpha\eta M}{\mu}\right) D_1 I_0\left(r\sqrt{\frac{s}{c}}\right) - \frac{2\mu M(1-\nu) - \alpha^2 M^2(1-2\nu)}{2\mu(1-\nu)} D_1 I_0\left(r_0\sqrt{\frac{s}{c}}\right). \tag{42}$$

We can now consider the two remaining stresses and the elastic displacement. The Laplace transformed  $\bar{\sigma}_{\theta\theta}$  can be written as

$$\bar{\sigma}_{\theta\theta} = -\frac{2\eta M}{r} \sqrt{\frac{c}{s}} D_1 I_1\left(r\sqrt{\frac{s}{c}}\right) - 2\eta M D_1 I_0\left(r\sqrt{\frac{s}{c}}\right) + \frac{2\mu}{1-2\nu} \bar{B}_1(s), \tag{43}$$

where again we note that for the solution to be bounded at  $r = 0$ , we have dropped the term associated with  $B_2(t)$ . Then, finally, the transformed  $\bar{\sigma}_{zz}$  is given by

$$\bar{\sigma}_{zz} = -2\eta M D_1 I_0\left(r\sqrt{\frac{s}{c}}\right) + \frac{4\mu\nu}{1-2\nu} \bar{B}_1(s), \tag{44}$$

and the transformed elastic displacement  $\bar{u}_r$  is

$$\bar{u}_r = \frac{\eta M}{\mu} \sqrt{\frac{c}{s}} D_1 I_1\left(r\sqrt{\frac{s}{c}}\right) + \bar{B}_1(s)r, \tag{45}$$

where again we note that for the solution to be bounded at  $r = 0$ , we have omitted the term associated with  $B_2(t)$ . Now, as before, using the expression for  $\bar{B}_1$  and Eqs. (43), (44), and (45), one obtains that

$$\begin{aligned} \bar{\sigma}_{\theta\theta} = & -\frac{2\eta M}{r} \sqrt{\frac{c}{s}} D_1 I_1\left(r\sqrt{\frac{s}{c}}\right) + \frac{2\mu(1-\nu) - \alpha^2 M(1-2\nu)}{2\alpha(1-2\nu)(1-\nu)} D_1 I_0\left(r_0\sqrt{\frac{s}{c}}\right) \\ & - 2\eta M D_1 I_0\left(r\sqrt{\frac{s}{c}}\right), \end{aligned} \tag{46}$$

$$\bar{\sigma}_{zz} = -2\eta M D_1 I_0\left(r\sqrt{\frac{s}{c}}\right) + \frac{\nu(2\mu(1-\nu) - \alpha^2 M(1-2\nu))}{\alpha(1-2\nu)(1-\nu)} I_0\left(r_0\sqrt{\frac{s}{c}}\right) D_1, \tag{47}$$

$$\bar{u}_r = \frac{\eta M}{\mu} \sqrt{\frac{c}{s}} D_1 I_1\left(r\sqrt{\frac{s}{c}}\right) + \frac{2\mu(1-\nu) - \alpha^2 M(1-2\nu)}{4\mu\alpha(1-\nu)} D_1 I_0\left(r_0\sqrt{\frac{s}{c}}\right)r. \tag{48}$$

In summary, the solution in the Laplace transformed domain is given by  $\bar{p}$  (see Eq. (42)),  $\bar{\sigma}_{rr}$  (see Eq. (41)),  $\bar{\sigma}_{\theta\theta}$  (see Eq. (46)),  $\bar{\sigma}_{zz}$  (see Eq. (47)), and  $\bar{u}_r$  (see Eq. (48)). The next (and last) step is to convert this solution back to the time domain.

### 2.2 Solutions in the time domain

To obtain the solution in the time domain, we carry out the inverse Laplace transform. The inverse Laplace transform of a general function  $\bar{f}(s)$  can be expressed as the ratio of two analytic functions as  $\bar{f}(s) = h(s)/g(s)$ . If  $g(s)$  contains zeros at  $S_n^* = 1, 2, \dots, \infty$ , then, the Laplace inversion becomes

$$f(t) = \frac{1}{2\pi i} \int_{\gamma-i\infty}^{\gamma+i\infty} \bar{f}(s)e^{st} ds = \frac{1}{2\pi i} \oint_C \frac{h(s)}{g(s)} e^{st} ds = \sum_{n=1}^{\infty} \frac{h(S_n^*)}{g'(S_n^*)} e^{S_n^* t}. \tag{49}$$

## 2.2.1 Pressure

Using Eq. (42) and  $D_1$ , given by Eq. (39), the pressure can be written as

$$\begin{aligned} \bar{p} = & \left( -\alpha P_0 \sqrt{s} r_0 (1 - 2\nu) \left( 2\mu(1 - \nu) \left( I_0 \left( r \sqrt{\frac{s}{c}} \right) - M I_0 \left( r_0 \sqrt{\frac{s}{c}} \right) \right) \right. \right. \\ & \left. \left. - \alpha^2 M (1 - 2\nu) \left( I_0 \left( r \sqrt{\frac{s}{c}} \right) - M I_0 \left( r_0 \sqrt{\frac{s}{c}} \right) \right) \right) \right) / \left( \mu I_0 \left( r_0 \sqrt{\frac{s}{c}} \right) (2\sqrt{s} r_0 (1 - \nu) \mu \right. \right. \\ & \left. \left. - \alpha^2 M (1 - 2\nu) r_0 \sqrt{s} \right) - 2\mu \alpha^2 M (1 - 2\nu)^2 \sqrt{c} I_1 \left( r_0 \sqrt{\frac{s}{c}} \right) \right). \end{aligned} \quad (50)$$

Using the non-dimensionalized variables  $S^* = \frac{r_0^2 s}{c}$  and  $R^* = \frac{r}{r_0}$ , we can write the pressure expression as the ratio of two analytic functions,

$$\begin{aligned} \frac{h(S^*)}{g(S^*)} = & \left( -\alpha P_0 \sqrt{S^*} (1 - 2\nu) (2\mu(1 - \nu) (I_0(R^* \sqrt{S^*}) - M I_0(\sqrt{S^*})) \right. \\ & \left. - \alpha^2 M (1 - 2\nu) (I_0(R^* \sqrt{S^*}) - M I_0(\sqrt{S^*})) \right) / \left( \mu I_0(\sqrt{S^*}) (2\sqrt{S^*} (1 - \nu) \mu \right. \\ & \left. - \alpha^2 M (1 - 2\nu) \sqrt{S^*}) - 2\mu \alpha^2 M (1 - 2\nu)^2 I_1(\sqrt{S^*}) \right). \end{aligned} \quad (51)$$

In the time domain, we have

$$p = \sum_{n=1}^{\infty} \frac{h(S_n^*)}{g'(S_n^*)} e^{S_n t^*}, \quad (52)$$

where the  $n$  zeros are found from  $g(S^*) = 0$ , i.e.,

$$\mu I_0(\sqrt{S^*}) (2\sqrt{S^*} (1 - \nu) \mu - \alpha^2 M (1 - 2\nu) \sqrt{S^*}) - 2\mu \alpha^2 M (1 - 2\nu)^2 I_1(\sqrt{S^*}) = 0, \quad (53)$$

which can be solved numerically to find each  $S_n^*$  for  $n = 1, 2, \dots, \infty$ . Due to Eq. (52), one also needs to find

$$\begin{aligned} g'(S^*) = & (2(1 - \nu) \mu^2 - \mu \alpha^2 M (1 - 2\nu)) \left( \frac{I_0(\sqrt{S^*})}{2\sqrt{S^*}} + \frac{I_1(\sqrt{S^*})}{2} \right) \\ & - 2\mu \alpha^2 M (1 - 2\nu)^2 \left( \frac{I_0(\sqrt{S^*})}{2\sqrt{S^*}} - \frac{I_1(\sqrt{S^*})}{2S^*} \right) \\ = & ((2(1 - \nu) \mu^2 - \mu \alpha^2 M (1 - 2\nu)) (I_0(\sqrt{S^*}) \sqrt{S^*} + S^* I_1(\sqrt{S^*})) \\ & - 2\mu \alpha^2 M (1 - 2\nu)^2 (I_0(\sqrt{S^*}) \sqrt{S^*} - I_1(\sqrt{S^*}))) / (2S^*). \end{aligned} \quad (54)$$

Therefore, using Eqs. (52) and (54), one gets

$$\begin{aligned} p = & \sum_{n=1}^{\infty} \left( -2\alpha P_0 S_n^{3/2} (1 - 2\nu) (2\mu(1 - \nu) (I_0(R^* \sqrt{S_n^*}) - M I_0(\sqrt{S_n^*})) \right. \\ & \left. - \alpha^2 M (1 - 2\nu) (I_0(R^* \sqrt{S_n^*}) - M I_0(\sqrt{S_n^*})) \right) e^{S_n t^*} \\ & / \left( (2(1 - \nu) \mu^2 - \mu \alpha^2 M (1 - 2\nu)) (I_0(\sqrt{S_n^*}) \sqrt{S_n^*} + S_n^* I_1(\sqrt{S_n^*})) \right. \\ & \left. - 2\mu \alpha^2 M (1 - 2\nu)^2 (I_0(\sqrt{S_n^*}) \sqrt{S_n^*} - I_1(\sqrt{S_n^*})) \right), \end{aligned} \quad (55)$$

where  $t^* = \frac{ct}{r_0^2}$  is the non-dimensional time. We can then make the change of variables  $S_n^* = -x_n$ , and under these circumstances, the Bessel functions involved become  $J_0(R^* \sqrt{x_n})$ ,  $J_0(\sqrt{x_n})$ , and  $J_1(\sqrt{x_n})$ .

One finally can write the pressure in an isotropic porous cylinder in the time domain as

$$p = \sum_{n=1}^{\infty} (2\alpha P_0 x_n^{3/2} (1 - 2\nu) (2\mu(1 - \nu) (J_0(R^* \sqrt{x_n}) - MJ_0(\sqrt{x_n})) - \alpha^2 M(1 - 2\nu) (J_0(R^* \sqrt{x_n}) - MJ_0(\sqrt{x_n}))) e^{-x_n t^*}) / (\mu C(x_n)), \tag{56}$$

where

$$C(x_n) = (2(1 - \nu)\mu - \alpha^2 M(1 - 2\nu)) (J_0(\sqrt{x_n}) \sqrt{x_n} - x_n J_1(\sqrt{x_n})) - 2\alpha^2 M(1 - 2\nu)^2 (J_0(\sqrt{x_n}) \sqrt{x_n} - J_1(\sqrt{x_n})), \tag{57}$$

in which  $x_n$  are real and positive.

### 2.2.2 Stress $\sigma_{rr}$

We carry out the same procedure for  $\bar{\sigma}_{rr}$ . Beginning with Eq. (41) and substituting  $D_1$  (see Eq. (39)), we have

$$\bar{\sigma}_{rr} = \frac{P_0 r_0 (\alpha^2 M(1 - 2\nu) (2(1 - 2\nu) I_1(r \sqrt{\frac{s}{c}}) \sqrt{c} - r I_0(r_0 \sqrt{\frac{s}{c}}) \sqrt{s}) + 2\mu r (1 - \nu) I_0(r_0 \sqrt{\frac{s}{c}}) \sqrt{s})}{r (I_0(r_0 \sqrt{\frac{s}{c}}) (2\sqrt{s} r_0 (1 - \nu) \mu - \alpha^2 M(1 - 2\nu) r_0 \sqrt{s}) - 2\alpha^2 M(1 - 2\nu)^2 \sqrt{c} I_1(r_0 \sqrt{\frac{s}{c}}))}. \tag{58}$$

Then, using the non-dimensionalized variables  $S^* = \frac{r_0^2 s}{c}$  and  $R^* = \frac{r}{r_0}$ , we can write this as the ratio of two analytic functions

$$\frac{h(S^*)}{g(S^*)} = (P_0 (\alpha^2 M(1 - 2\nu) (2(1 - 2\nu) I_1(R^* \sqrt{S^*}) - \sqrt{S^*} R^* I_0(\sqrt{S^*})) + 2\mu \sqrt{S^*} R^* (1 - \nu) (I_0(\sqrt{S^*}))) / (R^* (I_0(\sqrt{S^*}) (2\sqrt{S^*} (1 - \nu) \mu - \alpha^2 M(1 - 2\nu) \sqrt{S^*}) - 2\alpha^2 M(1 - 2\nu)^2 I_1(\sqrt{S^*}))). \tag{59}$$

Then, in the time domain, we have

$$\sigma_{rr} = \sum_{n=1}^{\infty} \frac{h(S_n^*)}{g'(S_n^*)} e^{S_n^* t^*}, \tag{60}$$

where  $n$  zeros are found from  $g(S^*) = 0$ , which can be solved numerically to find all the  $S_n^*$ . This will give the same zeros in Eq. (53). Due to Eq. (60), we also need to find  $g'(S^*)$ , which is given by  $\frac{R^*}{\mu} \times$  Eq. (54). Therefore, in the time domain, using (60), we have

$$\sigma_{rr} = \sum_{n=1}^{\infty} (2S_n^* P_0 (\alpha^2 M(1 - 2\nu) (2(1 - 2\nu) I_1(R^* \sqrt{S_n^*}) - \sqrt{S_n^*} R^* I_0(\sqrt{S_n^*})) + 2\mu \sqrt{S_n^*} R^* (1 - \nu) (I_0(\sqrt{S_n^*}))) e^{S_n^* t^*}) / (R^* (2(1 - \nu) \mu - \alpha^2 M(1 - 2\nu)) (I_0(\sqrt{S_n^*}) \sqrt{S_n^*} + S_n^* I_1(\sqrt{S_n^*}) - 2R^* \alpha^2 M(1 - 2\nu)^2 (I_0(\sqrt{S_n^*}) \sqrt{S_n^*} - I_1(\sqrt{S_n^*}))), \tag{61}$$

where  $t^* = \frac{ct}{r_0^2}$  is the non-dimensional time. We can then make the change of variables  $S_n^* = -x_n$  so that the Bessel functions involved become  $J_0(R^* \sqrt{x_n})$ ,  $J_0(\sqrt{x_n})$ , and  $J_1(\sqrt{x_n})$ .

We therefore find that the solution for  $\sigma_{rr}$  in the time domain is

$$\sigma_{rr} = \sum_{n=1}^{\infty} (-2x_n P_0 (\alpha^2 M(1 - 2\nu) (2(1 - 2\nu) J_1(R^* \sqrt{x_n}) - \sqrt{x_n} R^* J_0(\sqrt{x_n})) + 2\mu \sqrt{x_n} R^* (1 - \nu) (J_0(\sqrt{x_n}))) e^{-x_n t^*}) / (R^* C(x_n)). \tag{62}$$

### 2.2.3 Stress $\sigma_{\theta\theta}$

We consider the stress  $\sigma_{\theta\theta}$ . We begin with Eq. (46) and substitute  $D_1$  given by Eq. (39) to obtain

$$\begin{aligned} \bar{\sigma}_{\theta\theta} = & \left( P_0 r_0 \left( \alpha^2 M (1 - 2\nu) \left( 2(1 - 2\nu) \left( I_1 \left( r \sqrt{\frac{s}{c}} \right) \sqrt{c} - r I_0 \left( r \sqrt{\frac{s}{c}} \right) \sqrt{s} \right) - r I_0 \left( r_0 \sqrt{\frac{s}{c}} \right) \sqrt{s} \right) \right. \right. \\ & + 2\mu r (1 - \nu) I_0 \left( r_0 \sqrt{\frac{s}{c}} \right) \sqrt{s} \left. \right) / \left( r \left( I_0 \left( r_0 \sqrt{\frac{s}{c}} \right) (2\sqrt{s} r_0 (1 - \nu) \mu - \alpha^2 M (1 - 2\nu) r_0 \sqrt{s}) \right. \right. \\ & \left. \left. - 2\alpha^2 M (1 - 2\nu)^2 \sqrt{c} I_1 \left( r_0 \sqrt{\frac{s}{c}} \right) \right) \right). \end{aligned} \quad (63)$$

Then, using the non-dimensionalized variables  $S^* = \frac{r_0^2 s}{c}$  and  $R^* = \frac{r}{r_0}$ , we can write the ratio of two analytic functions as

$$\begin{aligned} \frac{h(S^*)}{g(S^*)} = & \left( P_0 (\alpha^2 M (1 - 2\nu) (2(1 - 2\nu) (I_1(R^* \sqrt{S^*}) - \sqrt{S^*} R^* I_0(R^* \sqrt{S^*})) - \sqrt{S^*} R^* I_0(\sqrt{S^*})) \right. \\ & + 2\mu \sqrt{S^*} R^* (1 - \nu) (I_0(\sqrt{S^*}))) / (R^* (I_0(\sqrt{S^*}) (2\sqrt{S^*} (1 - \nu) \mu \\ & \left. - \alpha^2 M (1 - 2\nu) \sqrt{S^*}) - 2\alpha^2 M (1 - 2\nu)^2 I_1(\sqrt{S^*}))). \end{aligned} \quad (64)$$

It follows that in the time domain we have

$$\sigma_{\theta\theta} = \sum_{n=1}^{\infty} \frac{h(S_n^*)}{g'(S_n^*)} e^{S_n^* t^*}. \quad (65)$$

Since  $g(S^*)$  here is  $\frac{R^*}{\mu} \times$  Eq. (53), the zeros are the same as those found numerically from Eq. (53), and the derivatives are the same as those found for  $\sigma_{rr}$ . Therefore, in the time domain, we have

$$\begin{aligned} \sigma_{\theta\theta} = & \sum_{n=1}^{\infty} (2S_n^* P_0 (\alpha^2 M (1 - 2\nu) (2(1 - 2\nu) (I_1(R^* \sqrt{S_n^*}) - \sqrt{S_n^*} R^* I_0(R^* \sqrt{S_n^*})) \\ & - \sqrt{S_n^*} R^* I_0(\sqrt{S_n^*})) + 2\mu \sqrt{S_n^*} R^* (1 - \nu) (I_0(\sqrt{S_n^*}))) e^{S_n^* t^*} \\ & / (R^* (2(1 - \nu) \mu - \alpha^2 M (1 - 2\nu)) (I_0(\sqrt{S_n^*}) \sqrt{S_n^*} + S_n^* I_1(\sqrt{S_n^*})) \\ & - 2R^* \alpha^2 M (1 - 2\nu)^2 (I_0(\sqrt{S_n^*}) \sqrt{S_n^*} - I_1(\sqrt{S_n^*}))), \end{aligned} \quad (66)$$

where  $t^* = \frac{ct}{r_0^2}$  is the non-dimensional time. We can then make the change of variables  $S_n^* = -x_n$  so that the Bessel functions involved become  $J_0(R^* \sqrt{x_n})$ ,  $J_0(\sqrt{x_n})$ , and  $J_1(\sqrt{x_n})$ .

As before, one can finally write the stress  $\sigma_{\theta\theta}$  in the time domain as

$$\begin{aligned} \sigma_{\theta\theta} = & \sum_{n=1}^{\infty} \left( (-2x_n P_0 (\alpha^2 M (1 - 2\nu) (2(1 - 2\nu) (J_1(R^* \sqrt{x_n}) \right. \\ & - \sqrt{x_n} R^* J_0(R^* \sqrt{x_n})) - \sqrt{x_n} R^* J_0(\sqrt{x_n}))) / (R^* C(x_n)) \\ & \left. + \frac{2\mu \sqrt{x_n} R^* (1 - \nu) (J_0(\sqrt{x_n})) e^{-x_n t^*}}{R^* C(x_n)} \right). \end{aligned} \quad (67)$$

#### 2.2.4 Stress $\sigma_{zz}$

We now consider the stress  $\sigma_{zz}$ . We begin with Eq. (47) and substitute  $D_1$  given by Eq. (39) to obtain

$$\bar{\sigma}_{zz} = \frac{2P_0 r_0 \sqrt{s} (\alpha^2 M (1 - 2\nu) ((1 - 2\nu) I_0(r \sqrt{\frac{s}{c}}) + \nu I_0(r_0 \sqrt{\frac{s}{c}})) - 2\nu \mu (1 - \nu) I_0(r_0 \sqrt{\frac{s}{c}}))}{(I_0(r_0 \sqrt{\frac{s}{c}}) (2\sqrt{s} r_0 (1 - \nu) \mu - \alpha^2 M (1 - 2\nu) r_0 \sqrt{s}) - 2\alpha^2 M (1 - 2\nu)^2 \sqrt{c} I_1(r_0 \sqrt{\frac{s}{c}}))}. \quad (68)$$

Then, using the non-dimensionalized variables  $S^* = \frac{r_0^2 s}{c}$  and  $R^* = \frac{r}{r_0}$ , we can write as the ratio of two analytic functions,

$$\frac{h(S^*)}{g(S^*)} = \frac{2P_0 \sqrt{S^*} (\alpha^2 M (1 - 2\nu) ((1 - 2\nu) I_0(R^* \sqrt{S^*}) + \nu I_0(\sqrt{S^*})) - 2\nu \mu (1 - \nu) (I_0(\sqrt{S^*})))}{(I_0(\sqrt{S^*}) (2\sqrt{S^*} (1 - \nu) \mu - \alpha^2 M (1 - 2\nu) \sqrt{S^*}) - 2\alpha^2 M (1 - 2\nu)^2 I_1(\sqrt{S^*}))}. \quad (69)$$

Then, in the time domain, we have that where  $n$  zeros are found from  $g(S^*) = 0$ , which can be solved numerically to find all the  $S_n^*$ . This will give the same zeros as in Eq. (53). Due to Eq. (60) we also need to find  $g'(S^*)$ , which is given by  $\frac{1}{\mu} \times$  Eq. (54). Therefore, in the time domain, we have

$$\begin{aligned} \sigma_{zz} = & \sum_{n=1}^{\infty} (2\sqrt{S_n^*} P_0 (\alpha^2 M (1 - 2\nu) ((1 - 2\nu) I_0(R^* \sqrt{S_n^*}) + \nu I_0(\sqrt{S_n^*})) \\ & - 2\nu \mu (1 - \nu) (I_0(\sqrt{S_n^*})) e^{S_n^* t^*}) / ((2(1 - \nu) \mu - \alpha^2 M (1 - 2\nu)) (I_0(\sqrt{S_n^*}) \sqrt{S_n^*} \\ & + S_n^* I_1(\sqrt{S_n^*})) - 2\alpha^2 M (1 - 2\nu)^2 (I_0(\sqrt{S_n^*}) \sqrt{S_n^*} - I_1(\sqrt{S_n^*}))), \end{aligned} \tag{70}$$

where  $t^* = \frac{ct}{r_0^2}$  is the non-dimensional time. We can then make the change of variables  $S_n^* = -x_n$  so that the Bessel functions involved become  $J_0(R^* \sqrt{x_n})$ ,  $J_0(\sqrt{x_n})$ , and  $J_1(\sqrt{x_n})$ .

We therefore have

$$\begin{aligned} \sigma_{zz} = & \sum_{n=1}^{\infty} (2\sqrt{x_n} P_0 (\alpha^2 M (1 - 2\nu) ((1 - 2\nu) J_0(R^* \sqrt{x_n}) + \nu J_0(\sqrt{x_n})) \\ & - 2\nu \mu (1 - \nu) (J_0(\sqrt{x_n})) e^{-x_n t^*}) / (C(x_n)), \end{aligned} \tag{71}$$

where  $\sigma_{zz}$  is the stress in the time domain.

### 2.2.5 Displacement $u_r$

Finally, we can consider the displacement  $u_r$ . We begin with  $\bar{u}_r$  (see Eq. (48)) and substitute  $D_1$  (see Eq. (39)) to obtain

$$\begin{aligned} \bar{u}_r = & \left( -P_0 r_0 (1 - 2\nu) \left( \alpha^2 M (1 - 2\nu) \left( 2\sqrt{c} I_1 \left( r \sqrt{\frac{s}{c}} \right) - r \sqrt{s} I_0 \left( r_0 \sqrt{\frac{s}{c}} \right) \right) \right. \right. \\ & \left. \left. + 2\mu (1 - \nu) \sqrt{s} r I_0 \left( r_0 \sqrt{\frac{s}{c}} \right) \right) \right) / \left( 2\mu \left( I_0 \left( r_0 \sqrt{\frac{s}{c}} \right) (2\sqrt{s} r_0 (1 - \nu) \mu \right. \right. \right. \\ & \left. \left. - \alpha^2 M (1 - 2\nu) r_0 \sqrt{s} \right) - 2\alpha^2 M (1 - 2\nu)^2 \sqrt{c} I_1 \left( r_0 \sqrt{\frac{s}{c}} \right) \right). \end{aligned} \tag{72}$$

Then, using the non-dimensionalized variables  $S^* = \frac{r_0^2 s}{c}$  and  $R^* = \frac{r}{r_0}$ , we can write as the ratio of two analytic functions,

$$\begin{aligned} \frac{h(S^*)}{g(S^*)} = & (-P_0 r_0 (1 - 2\nu) (\alpha^2 M (1 - 2\nu) (2I_1(R^* \sqrt{S^*}) - R^* \sqrt{S^*} I_0(\sqrt{S^*})) \\ & + 2\mu (1 - \nu) R^* \sqrt{S^*} I_0(\sqrt{S^*})) / (2\mu (I_0(\sqrt{S^*}) (2\sqrt{S^*} (1 - \nu) \mu \\ & - \alpha^2 M (1 - 2\nu) \sqrt{S^*}) - 2\alpha^2 M (1 - 2\nu)^2 I_1(\sqrt{S^*}))). \end{aligned} \tag{73}$$

Then, in the time domain, we have

$$u_r = \sum_{n=1}^{\infty} \frac{h(S_n^*)}{g'(S_n^*)} e^{S_n^* t^*}, \tag{74}$$

where  $n$  zeros are found from  $g(S^*) = 0$ , which can be solved numerically to find all the  $S_n^*$ . This will give the same zeros as in Eq. (53). Due to Eq. (60), we also need to find  $g'(S^*)$ , which is given by  $2 \times$  Eq. (54). In the time domain, one has

$$\begin{aligned} u_r = & \sum_{n=1}^{\infty} (-P_0 r_0 (1 - 2\nu) (\alpha^2 M (1 - 2\nu) (2I_1(R^* \sqrt{S_n^*}) - R^* \sqrt{S_n^*} I_0(\sqrt{S_n^*})) \\ & + 2\mu (1 - \nu) R^* \sqrt{S_n^*} I_0(\sqrt{S_n^*})) e^{S_n^* t^*}) / ((2(1 - \nu) \mu^2 - \mu \alpha^2 M (1 - 2\nu)) (I_0(\sqrt{S_n^*}) \sqrt{S_n^*} \\ & + S_n^* I_1(\sqrt{S_n^*})) - 2\mu \alpha^2 M (1 - 2\nu)^2 (I_0(\sqrt{S_n^*}) \sqrt{S_n^*} - I_1(\sqrt{S_n^*}))), \end{aligned} \tag{75}$$

where  $t^* = \frac{ct}{r_0^2}$  is the non-dimensional time. We can then make the change of variables  $S_n^* = -x_n$  so that the Bessel functions involved become  $J_0(R^* \sqrt{x_n})$ ,  $J_0(\sqrt{x_n})$ , and  $J_1(\sqrt{x_n})$ .

We therefore have

$$u_r = \sum_{n=1}^{\infty} (-P_0 r_0 (1 - 2\nu) (\alpha^2 M (1 - 2\nu) (2J_1(R^* \sqrt{x_n}) - R^* \sqrt{x_n} J_0(\sqrt{x_n})) + 2\mu(1 - \nu) R^* \sqrt{x_n} J_0(\sqrt{x_n})) e^{-x_n t^*}) / (\mu C(x_n)), \quad (76)$$

where  $u_r$  is the displacement in an isotropic porous elastic cylinder in the time domain.

In summary, the full analytical solution for the pressure, stresses and elastic displacement of an isotropic porous cylinder is given by  $p$  (see Eq. (56)),  $\sigma_{rr}$  (see Eq. (62)),  $\sigma_{\theta\theta}$  (see Eq. (67)),  $\sigma_{zz}$  (see Eq. (71)), and  $u_r$  (see Eq. (76)).

### 2.3 Simplification of the pressure for the sensitivity analysis

In this work, we focus on the sensitivity analysis of the parameters involved in the expression for the pressure (56). As the expression of pressure is a sum evaluated for each  $x_n$ , for  $n = 1, 2, \dots, \infty$ , which are zeros of the expression (53), we have a very lengthy expression. Therefore, before carrying out the sensitivity analysis, we need to simplify the pressure sum. We do this by considering only the first 5 terms of the expanded sum (see Eq. (56)). To expand the sum, we need to calculate the first 5 zeros of expression (53), where we assume that the parameters are not varying.

The parameters that we require are the standard poroelastic parameters. The parameter  $\mu$  is the shear modulus, and hence it has the unit of pressure,  $M$  is Biot's modulus, and therefore also has the unit of pressure. The Poisson ratio  $\nu$  is non-dimensional, and so is Biot's coefficient  $\alpha$ . These are standard poroelastic coefficients as discussed in Refs. [17], [21], [50], and [53]. In porous media, the Poisson ratio  $\nu$  is confined to a range (0, 1), where this range means that the material goes from fully compressible to incompressible. Biot's modulus  $M$  approaching infinity, together with Biot's coefficient  $\alpha$  approaching 1, represents a situation that would be achieved for the intrinsic incompressibility of the matrix. Therefore, we choose  $\mu = 1$  and  $M = 50\,000$ , which can be taken to represent that  $M$  is therefore approaching infinity. We want to consider a porous material that has an intrinsically incompressible solid matrix. Therefore, we have chosen  $\mu = 1$ ,  $\nu = 0$ ,  $\alpha = 1$ , and  $M = 50\,000$  to calculate  $x_n$ .

We then find the first 5  $x_n$ , which are

$$x_n = (8.7002, 34.119, 78.726, 142.95, 226.88). \quad (77)$$

In Fig. 2, we plot the solution to  $p$  (see Eq. (56)) using the first five  $x_n$  that have been obtained. Since we have a smooth profile, we can conclude that the first five  $x_n$  values are sufficient to determine the behavior of the pressure. We are now able to carry out the sensitivity analysis on the parameters of Eq. (56) evaluated at the first five  $x_n$ . The expanded expression with which we carry out the sensitivity analysis is given in Appendix A.

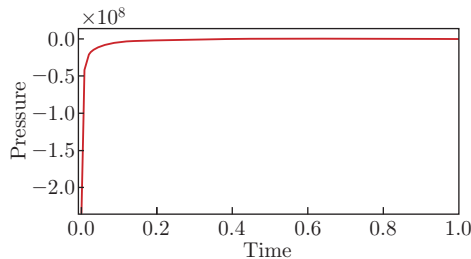


**Fig. 2** Pressure profile for the porous cylinder using the first five  $x_n$  (color online)

### 3 On the sensitivity analysis

Sensitivity analysis examines the effect of input parameters on output variables in a model. Researchers need to determine the contribution of uncertainty for each involved input parameter on the output of the model. If the input parameters follow relevant probability distributions, statistical methods can be used to understand the parameters that contribute to the variability of the model output.

Sensitivity analysis can be either deterministic or probabilistic. In a deterministic sensitivity analysis approach, we have a predefined fixed value for each of the parameters, while in the probabilistic sensitivity analysis methods, we consider a range of accepted values for each input parameter. Since in this work we are dealing with porous media, the input parameters have a range of possible values; therefore, the probabilistic approach is a more appropriate choice.

In what follows, we consider the Sobol method due to the nature of the problem. In Subsection 3.1, we recap the Sobol method. In Subsection 3.2, the three probability distributions, namely, the uniform, exponential, and Weibull, applied to the problem at hand are reviewed. Subsection 3.3 considers the assessments of the Sobol method using both the bias measure and the standard deviation.

#### 3.1 Sobol method

The Sobol method is defined as a numerical method<sup>[20]</sup>, and it is a variance-based sensitivity analysis that is categorized as a statistical approach in sensitivity analysis methods. This method figures out the impact of contributed variations of the input parameters on the output variables of the model<sup>[22]</sup>. Through variance-based computation, the amount of uncertainty of the output variable of the model is determined with attention to the contribution of individual input parameters and their interactions<sup>[38]</sup>.

Assume, in a general notation, the random vector  $X = (X_1, X_2, \dots, X_t)$  ( $X_i$  are the input variables), and  $y = f(X)$  (i.e.,  $y$  is the output). Furthermore, suppose that  $f(\cdot)$  is a function<sup>[22]</sup> that is defined on the interval  $[0, 1]^t$  as

$$f(X) = f_0 + \sum_{i=1}^t f_i(X_i) + \sum_{i<j}^t f_{ij}(X_i, X_j) + \dots + f_{12\dots t}(X), \tag{78}$$

where

$$\int_0^1 f_{i_1\dots i_s}(X_{i_1}, X_{i_2}, \dots, X_{i_s}) dx_{i_l} = 0, \quad 1 \leq l \leq s, \quad \{i_1, i_2, \dots, i_s\} \subseteq \{1, 2, \dots, t\}. \tag{79}$$

In accordance to functional analysis of variance, the variance of a function is given as<sup>[39]</sup>

$$\text{Var}(y) = \sum_{i=1}^t D_i(y) + \sum_{i<j}^t D_{ij}(y) + \dots + D_{12\dots t}(y), \tag{80}$$

where  $D_i(y) = \text{Var}(E(y | X_i))$  are the first-order indices, and  $E$  is the mathematical expectation for  $(y | X_i, X_j)$ ; likewise,  $D_{ij}(y) = \text{Var}(E(y | X_i, X_j)) - D_i(y) - D_j(y)$  are the second-order indices, etc. The first-order indices and second-order interaction indices are gained as<sup>[40]</sup>

$$S_{y_i} = \frac{D_i(y)}{\text{Var}(y)}, \quad S_{ij} = \frac{D_{ij}(y)}{\text{Var}(y)}, \tag{81}$$

respectively. There are  $2^t - 1$  indices computed using this method. For instance, if one considers seven input variables, i.e.,  $t = 7$ , there are  $2^7 - 1 = 127$  indices including individual and interaction effects in the model. The following total indices are proposed by Archer et al.<sup>[41]</sup>:

$$S_{T_i} = S_{y_i} + \sum_{i<j} S_{ij} + \sum_{j \neq i, l \neq i, j < l} S_{ijl} + \dots = \sum_{l \in \#i} S_l, \tag{82}$$

where  $\#i$  refers to all the subsets of  $\{1, 2, \dots, t\}$  that include the index  $i$ . The determination of the sampling design and an estimator is a necessary step to obtain variance-based sensitivity indices. In the case of the sampling design, Monte Carlo sampling-based methods for the first-order and interaction indices have been proposed by Sobol<sup>[42]</sup>. This approach has been further developed for both the first-order and total-order indices by Saltelli<sup>[40]</sup>. In addition, to calculate the error estimation for the indices, the combination of the Monte-Carlo method with the use of asymptotic formulas<sup>[43]</sup>, bootstrap methods<sup>[41]</sup>, and random repetition<sup>[44]</sup> has been used. Other estimators to obtain the first-order and total-order Sobol indices have been proposed, and we refer to the literature for details. Here, two estimators are used: the ‘‘Saltelli estimator’’<sup>[45]</sup> for the first-order effect, and the ‘‘Janson estimator’’<sup>[46]</sup> for the total sensitivity indices, which are proposed by Saltelli et al.<sup>[45]</sup> and Puy et al.<sup>[47]</sup>, respectively, since they can handle even non-monotonic and non-linear models.

For the first-order indices, the Saltelli estimator is

$$S_i = \frac{\frac{1}{t} \sum_{j=1}^t f(B)_j (f(A_B^{(i)})_j - f(A)_j)}{\text{Var}(y)}, \quad (83)$$

which is composed of combinations of the matrices  $A$ ,  $B$ ,  $A_B^{(i)}$ , or  $B_A^{(i)}$  (for the full description of these matrices, we refer to Ref. [47]). For the total indices, the Janson estimator is

$$T_i = \frac{\frac{1}{2t} \sum_{j=1}^t (f(A)_j - f(A_B^{(i)})_j)^2}{\text{Var}(y)}. \quad (84)$$

These estimators are obtained through a sampling-based approach in the model.  $T_i - S_i$  measures the joint effect of an input variable with attention to the interpretation of Sobol indices. In particular, it captures the uncertainty of a model due to the joint effects of the input  $X_i$  with other input parameters. It follows that if  $T_i = 0$ , then  $X_i$  does not have any total effect in the output of the model, and it is therefore not an influential input<sup>[46]</sup>.

We gain the second-order interactions defined in Eq. (81) using Liu and Owen’s formula<sup>[48]</sup> that expresses the higher-order interaction between two input parameters on the model output. The estimations of the second-order interactions are

$$\begin{aligned} \widehat{S}_{i,j} = & \frac{1}{4n} \sum_{t=1}^n (f(X_i^t, X_j^t, X_{-i,j}^t) - f(X_i^t, W_j^t, X_{-i,j}^t) \\ & - f(W_i^t, X_j^t, X_{-i,j}^t) + f(W_i^t, W_j^t, X_{-i,j}^t))^2, \end{aligned} \quad (85)$$

where the two independent copies defined on the interval  $[0, 1]^m$  from  $X_i$  and  $X_j$  are  $W_i$  and  $W_j$ , respectively,  $t$  is the number of repetitions in model output, and  $n$  is the sample size of input parameters. In addition,  $X_{-i,j}$  shows the interaction effect of two input parameters without the direct effect for  $X_{i,j}$  parameters, i.e., Eq. (85) is the estimation of the expected values of the joint effects of two input parameters on the output of the model. We represent the results of the joint effects of input parameters on model output using a scatter plot matrix. Scatter plots for some (we take three) input parameters on the pressure relation have been obtained in Section 4. In the scatter plots, the values of input parameters have been taken based on physical meaning.

Here, three different probability distributions, namely, uniform, exponential, and Weibull, are used to obtain the Sobol indices of the input parameters through ‘‘Saltelli-Jansen’’ estimators (see Eqs. (83) and (84)). Instead of having just random data or deterministic fixed data, we run statistical simulations in the ‘‘R’’ programming language as input values.

### 3.2 The applied probability distributions in the sensitivity analysis

The probability distribution function includes all possible values for a random variable (parameter)<sup>[49]</sup>. The inputs of our isotropic porous solid cylinder are distributed throughout a

specific range that affects the output variable (herein, pressure), i.e., results are susceptible to different input parameter distributions. Three probability distributions are considered for the input parameters: the uniform, exponential, and Weibull distributions. The domain for each input parameter is taken to be aligned with physical data for each distribution.

### 3.2.1 Uniform distribution

A continuous uniform distribution gives events that have the same chance to occur. It is described by two scalar features associated with a variable  $X$ : a minimum value  $a$  and a maximum value  $b$ . The probability density function of the uniform distribution is<sup>[20]</sup>

$$f(X) = \begin{cases} \frac{1}{b-a} & \text{for } a < X < b, \\ 0 & \text{for } X < a \text{ or } X > b. \end{cases} \tag{86}$$

Equation (86) is represented as a rectangular distribution function. The uniform distribution of a variable  $X$  is denoted as  $X \sim U(a, b)$ .

### 3.2.2 Exponential distribution

Another continuous probability distribution is the exponential distribution, which often concerns the values of a parameter until some specific event happens. It is a process in which events occur independently for a variable and continuously at a fixed mean rate. The lack of memory is the key property of the exponential distribution<sup>[49]</sup>, i.e., the past behavior of a parameter does not affect its future behavior. The application of this distribution is in economics, medicine, and many aspects of engineering fields. A random variable,  $X$ , follows the exponential distribution if the probability density function is

$$f(X) = \begin{cases} \theta e^{-\theta X} & \text{for } X > 0, \\ 0 & \text{for } X \leq 0. \end{cases} \tag{87}$$

The exponential distribution of a variable  $X$  is denoted as  $X \sim \exp(\theta)$ .

### 3.2.3 Weibull distribution

The Weibull distribution is mostly applied in the modeling of lifetime data in a process. In statistics and probability theory, the Weibull distribution is defined as a continuous probability distribution. The various applications of this distribution are mostly used in cases of time between events and also for considered failure times. For instance, the time a user spends surfing the web or the maximum one-day rainfall follows the Weibull distribution. The Weibull distribution is

$$f(X) = \beta \alpha (\beta X)^{\alpha-1} e^{-(\beta X)^\alpha} \quad \text{for } X > 0. \tag{88}$$

The Weibull distribution is applied in different types of engineering fields, such as radar systems, to simulate the dispersion of the received signal and to model stochastic processes related to the time of manufacturing. In this work, we consider the scale parameter of the Weibull distribution to be equal to one ( $\beta = 1$ ), the same that is given by default in the ‘‘R’’ program. The Weibull distribution of a variable  $X$  is denoted as  $X \sim W(\alpha, \beta)$  or simply as  $X \sim W(\alpha, 1)$ .

## 3.3 Statistical measurements for assessment of the results

To evaluate the robustness and quality of the results, the bias measure and standard deviation measure are applied. The bias measure is shown as<sup>[20]</sup>

$$\text{bias}(T) = \mathbb{E}[T] - O, \tag{89}$$

where  $O$  is a variable in a model,  $T$  is an estimation of  $O$ , and  $\mathbb{E}[T]$  is the mathematical expectation of  $T$ .  $\mathbb{E}[T]$  is the sum of all possible values for a random variable  $X$ , which is given by

$$\mathbb{E}[T] = \int_{-\infty}^{\infty} X f(X) dX. \tag{90}$$

Another assessment measure is the standard deviation, denoted by  $\sigma$ , which is

$$\sigma = \sqrt{\frac{1}{N-1} \sum_{i=1}^N (X_i - \bar{X})^2}, \quad (91)$$

where  $X$  is a random variable in the model,  $\bar{x}$  is the mean of  $X$ , and  $N$  is the sample size of the data.

In what follows, we apply the Sobol method to the pressure (output variable) described within the context of the problem in Section 2.

#### 4 Applications of the Sobol method

The Sobol method investigates how much the contribution of each input parameter can affect the uncertainty of the output variable in the model. The amount of contribution can be directly related to each input parameter (the first-order) or can come from the higher-order interactions between input parameters on the model output. In the Sobol method, two main indices are considered: the direct uncertainty impact of each input parameter, or the first-order index given by Eq. (81), and the total Sobol index given by Eq. (82), which computes the sum of all direct and indirect contributions of uncertainty for each input parameter in the model. The road map for applying the Sobol method to the problem at hand is divided into five steps.

(i) First, one needs to specify the input parameters in the model and assign the corresponding ranges for each input parameter.

(ii) Then, one runs the statistical simulation in the “R” program for each input parameter (sample size is  $N = 20\,000$ ) in the pressure relation (output).

(iii) After that, one obtains the sensitivity indices: by Saltelli-Janson estimators for the first-order indices using Eq. (83) and for total indices using Eq. (84).

(iv) With the results, one can sort out the sensitivity of the input parameters based on the highest value of the total indices.

(v) At last, assessment measures for the Sobol indices need to be obtained using the bias measure and standard deviation.

An auxiliary feature, namely the dummy parameter, is computed by the “R” program in the Sobol method for both the first-order and total Sobol indices. The dummy parameter gives us an insight to discriminate between influential and non-influential factors in the model. If the first (or total) Sobol index of an input parameter is less than the value of the first (or total) Sobol index given by the dummy parameter, then the input parameter is not influential for that output of the model. In addition, for each Sobol index, the confidence interval is considered based on 95% of the value of the index. The confidence interval is defined as  $C(I) = \bar{X} \pm Z \frac{s}{\sqrt{N}}$ , where  $Z$  is the confidence level value,  $\bar{X}$  is the sample mean,  $N$  is the sample size, and  $s$  is the sample standard deviation. Table 1 illustrates the range of each input parameter. The ranges are selected based upon typical physical ranges that could be related to porous media. Furthermore, Table 1 gives the possible ranges for the input parameters that follow the probability distributions based on their corresponding behavior in the model.

**Table 1** The ranges of the input parameters considered in Section 2 under various probability distributions for an isotropic porous solid cylinder

Parameter	$\mathcal{U}(a, b), \exp(\theta), \mathcal{W}(\alpha, 1)$	Parameter	$\mathcal{U}(a, b), \exp(\theta), \mathcal{W}(\alpha, 1)$
$\alpha$	$\mathcal{U}(0, 0.9)$	$M$	$\exp(1)$
$P_0$	$\mathcal{U}(70, 100)$	$t^*$	$\mathcal{W}(0.1, 1)$
$\nu$	$\mathcal{U}(0, 0.5)$	$R^*$	$\mathcal{U}(3, 25)$
$\mu$	$\mathcal{U}(0.1, 50)$		

Here, we have assigned the uniform distribution to parameters that have a specified (small)

range of accepted values, where the outcome of any of these values is equally likely, i.e., the parameters  $\alpha, \mu, \nu, R^*$ , and  $P_0$ . In addition, for the time parameter  $t^*$ , we adopt the Weibull distribution, as this is classically chosen to describe time to failure or time between events in a model. Finally, the exponential distribution is assigned to the parameter  $M$ , due to the large range of values and the physical behavior of Biot’s modulus in porous media, where  $M$  is monotonically increasing to infinity.

The results of Sobol indices, the first-order and total Sobol indices, are shown in Table 2. Based on the results, time  $t^*$  is the most sensitive input parameter to the output of the model (pressure) for both the first-order indices  $S_i$  and total indices  $T_i$ . Biot’s modulus  $M$  is the second most sensitive input parameter to the pressure. On the other hand, the initial pressure  $P_0$  is the least influential factor on the pressure output.

**Table 2** The first-order index ( $S_i$ ) and total Sobol index ( $T_i$ ) for the involved input parameters on the pressure  $p$  based on the range of inputs shown in Table 1

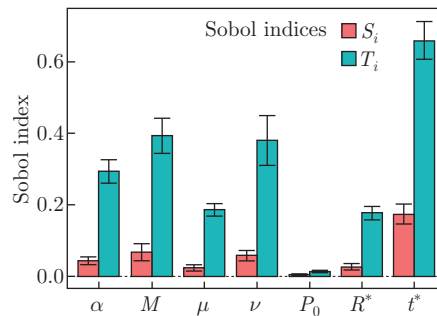
Parameter	$\mathcal{U}(a, b), \exp(\theta), \mathcal{W}(\alpha, 1)$	
	$S_i$	$T_i$
$\alpha$	0.046 047 89	0.276 587 78
$P_0$	0.011 664 61	0.056 609 42
$\nu$	0.018 448 65	0.358 260 83
$\mu$	0.084 121 09	0.176 129 23
$M$	0.177 103 03	0.370 199 92
$t^*$	0.230 709 73	0.621 690 59
$R^*$	0.060 189 95	0.167 438 31

Figure 3 shows the bar plots of Sobol indices in the model (those values are given in Table 2). The first-order index for the dummy parameter is indicated with a dashed horizontal red line, while the total index associated with the dummy parameter is indicated with a dashed horizontal blue line. Based on the results of the dummy parameter, all the input parameters, except  $P_0$  which is associated with indices lower than the ones of the dummy parameter, are influential factors for the pressure model. Based on the total Sobol indices, sorting out from the highest sensitive parameters to the lowest ones yields  $T_{t^*} > T_M > T_\nu > T_\alpha > T_\mu > T_{R^*} > T_{P_0}$ . The analytical solution in Subsection 2.2 is time-dependent as opposed to a time independent one. The sensitivity analysis captures this feature and gives the parameter time as the most influential one followed by the other inputs. For each Sobol index, the confidence interval is computed. This interval is illustrated in Fig. 3 as the values between the two parallel horizontal lines at the top of each index.

The assessment of Sobol indices is given using both bias measure and standard deviation measure. Results are shown in Tables 3 and 4. All values of both bias and standard deviation for both  $S_i$  and  $T_i$  are very small. It follows that Sobol indices for the internal pressure model are reliable.

For completeness, we consider now interaction effects among input parameters. For that purpose, we take three parameters since the results are shown as a scatter plot matrix. Figure 3 shows that the first-order effect of the parameter  $t^*$  is much higher than the first-order effect of the other parameters. For that reason, we do not consider the interaction effect between  $t^*$  and other input parameters in the model. The analysis has already captured the importance of  $t^*$  both by itself and interacting with the other parameters. On the other hand, we want to establish now the importance of the interaction among other parameters. Figure 4 shows the joint interaction effects among three sensitive input parameters ( $\alpha, \nu$ , and  $M$ ) on the pressure relation in a multi-scatter plot. The variable  $y$  indicates the pressure relation in the model (the output variable).

In Fig. 4, the patterns of the sensitivity of the model due to the joint effect between two



**Fig. 3** The Sobol indices for each input parameter in the pressure response of an isotropic porous cylinder subject to radial stress boundary conditions using “Saltelli-Jansen” estimators based on the range of inputs given in Table 1. The horizontal (blue and red) lines give the Sobol indices of the dummy parameter. If a (first-order or total) Sobol index for an input parameter is below the corresponding line (first or total) of the dummy parameter, then that input is not an influential factor on the output of the model. This only happens for  $P_0$  (color online)

**Table 3** Bias measures for the Sobol indices of the input parameters given in Table 1 associated with pressure  $p$

Bias measures Parameter	$\mathcal{U}(a, b), \exp(\theta), \mathcal{W}(\alpha, 1)$	
	$S_i$	$T_i$
$\alpha$	0.006 674 375	$-2.798\,784 \times 10^{-4}$
$P_0$	0.005 042 454	$1.653\,378 \times 10^{-5}$
$\nu$	0.005 800 765	$-2.131\,522 \times 10^{-3}$
$\mu$	0.007 166 889	$-8.217\,040 \times 10^{-4}$
$M$	0.009 140 604	$-2.582\,379 \times 10^{-3}$
$t^*$	0.006 296 964	$-1.231\,508 \times 10^{-3}$
$R^*$	0.004 150 855	$-2.310\,302 \times 10^{-3}$

**Table 4** Standard deviation measures for the Sobol indices of the input parameters given in Table 1 associated with pressure  $p$

Standard deviation Parameter	$\mathcal{U}(a, b), \exp(\theta), \mathcal{W}(\alpha, 1)$	
	$S_i$	$T_i$
$\alpha$	0.045 582 75	0.017 750 244 0
$P_0$	0.032 894 34	0.000 650 544 6
$\nu$	0.062 486 47	0.029 551 724 4
$\mu$	0.046 911 82	0.007 903 925 4
$M$	0.050 535 69	0.019 783 678 5
$t^*$	0.047 531 48	0.026 353 293 5
$R^*$	0.036 036 12	0.009 259 260 3

input parameters are as follows, keeping in mind that green dots are related to high interaction effect. There are significant green dots between  $\alpha$  and the two other inputs on the internal pressure due to the yellow-green colors (greater interaction) concentrated on the left side of the plots. These joint effects between  $\alpha$  and  $M$  as well as  $\alpha$  and  $\nu$  are clear in their corresponding plots for values of  $\alpha < 0.5$ . This implies that under these conditions one must concentrate on total Sobol indices values for these parameters to understand their importance in the model (the first-order index is much lower than the total Sobol index for these three parameters). It follows that for other values of  $\alpha$ , the important interaction effects are given by other parameters.

The interactions of Poisson’s ratio  $\nu$  and Biot’s modulus  $M$  give a mix of all colors with no pattern emerging. This means that these parameters have little interaction with each other. We

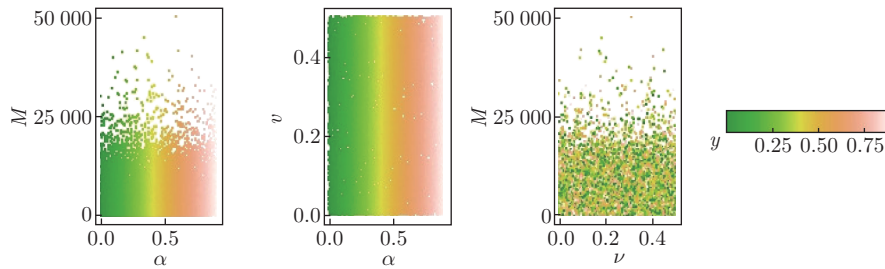


**Fig. 4** Interaction impact of Sobol indices for three influential parameters in the pressure relation  $p$ . The variable  $y$  is the model output representing the pressure (color online)

should note that the absence of interaction effect between Poisson's ratio and Biot's modulus can be attributed to the fact that we are carrying out an undrained analysis. In the case of a drained analysis, such as the one carried out in Ref. [50], it has been shown that Biot's modulus is monotonically increasing with regard to Poisson's ratio, and therefore, under these circumstances, one would indeed see the joint effects between those parameters.

## 5 Conclusions

In this work, we find an analytical solution to the equations that describe the mechanical behavior of a porous material. We investigate a solid cylinder with a microstructure comprising a porous elastic matrix, which is assumed to be isotropic. Materials with this microstructure have many real-world applications, including the modeling of biological tissues such as bones.

We then investigate the pressure via a sensitivity analysis to determine the influence of several parameters on that particular output. The analysis captures that the time  $t^*$ , Biot's modulus  $M$ , and Poisson's ratio  $\nu$ , have the highest influence on the pressure, whereas the initial value of pressure  $P_0$  plays very little role.

The current study is subject to some limitations and extensions that can increase the applicability of results. The models of poroelasticity from which we begin are the macroscale governing equations, as proposed by Biot, which were developed experimentally. However, it is possible to obtain the governing equations of poroelastic materials via homogenization techniques<sup>[51–53]</sup>. This would mean that a variety of different structural features such as pore geometry and arrangement, or even additional elastic or porous phases<sup>[54–55]</sup>, could be encoded in the effective elasticity tensor, which contributes to the stresses from which the analytic solution is obtained. The current solution has been developed assuming that the effective elasticity tensor modeling the cylinder is isotropic. It would also be possible to extend the analytic solution to more complicated symmetries such as cubic, tetragonal, or orthogonal symmetries, all of which could arise from using the asymptotic homogenization technique to obtain the governing equations. These different geometries could increase the applicability of such results, as they will be more realistic of biological scenarios.

The sensitivity analysis is carried out on the set of input parameters shown in Table 1, which are chosen based on a sampling design with a random approach and are not specific to any material. In future, it would be possible to choose a specific biological scenario such as bones. The bones have been modeled using a poroelastic approach<sup>[5,31–32]</sup>. The pores of bones are filled with bone marrow, blood, or interstitial fluid and cells<sup>[32–33]</sup>, and therefore would be a very good fit for the model proposed here. Soleimani et al.<sup>[35]</sup> stated that recent studies have provided evidence that the pressure and velocity of the interstitial fluid flowing in the pores of the bones play a significant role in the bone remodeling process<sup>[36–37]</sup>. Ghiasi et al.<sup>[36]</sup> also stated that the interstitial fluid velocity and the shear stress within the bones, which the interstitial velocity creates, may influence the cells responsible for bone healing. For this reason, the next steps in our analysis would be to carry out the same sensitivity analysis but

with input parameter ranges based upon bones to investigate the stresses.

It would also be possible to inform the parameter ranges via micromechanical simulations. If the model for of the poroelastic material was obtained via asymptotic homogenization, then we would have that the coefficients/parameters of the governing equations can be determined via solving porescale differential problems<sup>[50,56–57]</sup>. By solving these porescale differential problems, we could provide a range for each of the parameters to be used within the sensitivity analysis. This method would also allow the parameters to be tuned on the porescale geometry and mechanical properties.

Future sensitivity analyses can be implemented on some different scenarios corresponding to instability modes such as necking, bending, beading, helical buckling, bulging, and prismatic bifurcation<sup>[58–63]</sup>. Moreover, the material in biological soft tissue analysis is subjected to various biochemical and physical processes, and hence, the specifications of the constituents of the tissue may change, for example, due to remodeling mechanisms and growth<sup>[64–67]</sup>. Therefore, the study on the impact of these changes on the response of the structure is also another possible application of sensitivity analysis.

**Conflict of interest** The authors declare no conflict of interest.

**Open access** This article is licensed under a Creative Commons Attribution 4.0 International License, which permits use, sharing, adaptation, distribution and reproduction in any medium or format, as long as you give appropriate credit to the original author(s) and the source, provide a link to the Creative Commons licence, and indicate if changes were made. To view a copy of this licence, visit <http://creativecommons.org/licenses/by/4.0/>.

## References

- [1] BIOT, M. A. Theory of elasticity and consolidation for a porous anisotropic solid. *Journal of Applied Physics*, **26**(2), 182–185 (1955)
- [2] BIOT, M. A. General solutions of the equations of elasticity and consolidation for a porous material. *Journal of Applied Physics*, **23**(1), 91–96 (1956)
- [3] BIOT, M. A. Theory of propagation of elastic waves in a fluid-saturated porous solid, II: higher frequency range. *The Journal of the Acoustical Society of America*, **28**(2), 179–191 (1956)
- [4] BIOT, M. A. Mechanics of deformation and acoustic propagation in porous media. *Journal of Applied Physics*, **33**(4), 1482–1498 (1962)
- [5] COWIN, S. C. Bone poroelasticity. *Journal of Biomechanics*, **32**(3), 217–238 (1999)
- [6] WEINER, S. and WAGNER, H. D. The material bone: structure-mechanical function relations. *Annual Review of Materials Science*, **28**(1), 271–298 (1998)
- [7] COOKŠŌN, A., LEE, J., MICHLER, C., CHABINIOK, R., HYDE, E., NORDSLETTEN, D., SINCLAIR, M., SIEBES, M., and SMITH, N. A novel porous mechanical framework for modelling the interaction between coronary perfusion and myocardial mechanics. *Journal of Biomechanics*, **45**(5), 850–855 (2012)
- [8] MAY-NEWMAN, K. and MCCULLOCH, A. D. Homogenization modeling for the mechanics of perfused myocardium. *Progress in Biophysics and Molecular Biology*, **69**(2), 463–481 (1998)
- [9] BUKAC, M., YOTOV, I., ZAKERZADEH, R., and ZUNINO, P. *Effects of Poroelasticity on Fluid-Structure Interaction in Arteries: a Computational Sensitivity Study*, Springer International Publishing, Berlin, 197–220 (2015)
- [10] CHAPELLE, D., GERBEAU, J. F., SAINTE-MARIE, J., and VIGNON-CLEMENTEL, I. E. A poroelastic model valid in large strains with applications to perfusion in cardiac modeling. *Computational Mechanics*, **46**(1), 91–101 (2010)
- [11] BOTTARO, A. and ANSALDI, T. On the infusion of a therapeutic agent into a solid tumor modeled as a poroelastic medium. *Journal of Biomechanical Engineering*, **134**(8), 084501 (2012)
- [12] FLESSNER, M. F. The role of extracellular matrix in transperitoneal transport of water and solutes. *Peritoneal Dialysis International*, **21**(3), S24–S29 (2001)

- 
- [13] CHALASANI, R., POOLE-WARREN, L., CONWAY, R. M., and BEN-NISSAN, B. Porous orbital implants in enucleation: a systematic review. *Survey of Ophthalmology*, **52**(2), 145–155 (2007)
- [14] KARAGEORGIOU, V. and KAPLAN, D. Porosity of 3D biomaterial scaffolds and osteogenesis. *Biomaterials*, **26**(27), 5474–5491 (2005)
- [15] KÜMPPEL, H. J. Poroelasticity: parameters reviewed. *Geophysical Journal International*, **105**(3), 783–799 (1991)
- [16] WANG, H. F. *Theory of Linear Poroelasticity with Applications to Geomechanics and Hydrogeology*, Princeton University Press, Princeton (2017)
- [17] CHENG, A. H. D. *Analytical Solution*, Springer International Publishing, Berlin, 229–396 (2016)
- [18] LEEUW, D. The theory of three-dimensional consolidation applied to cylindrical bodies. *Proceeding of the 6th ICSMFE*, Shanghai (1965)
- [19] CARCIONE, J. M., MORENCY, C., and SANTOS, J. E. Computational poroelasticity: a review. *Geophysics*, **75**(5), 75A229–75A243 (2010)
- [20] SALTELLI, A., RATTO, M., ANDRES, T., CAMPOLONGO, F., CARIBONI, J., GATELLI, D., SAISANA, M., and TARANTOLA, S. *Global Sensitivity Analysis: the Primer*, John Wiley and Sons, New York (2008)
- [21] MEI, C. and VERNESCU, B. *Homogenization Methods for Multiscale Mechanics*, World Scientific, Singapore (2010)
- [22] SALTELLI, A., TARANTOLA, S., and CHAN, K. S. A quantitative model-independent method for global sensitivity analysis of model output. *Technometrics*, **41**(1), 39–56 (1999)
- [23] ANSTETT-COLLIN, F., MARA, T., and BASSET, M. Application of global sensitivity analysis to a tire model with correlated inputs. *Simulation Modelling Practice and Theory*, **44**, 54–62 (2014)
- [24] SAISANA, M., SALTELLI, A., and TARANTOLA, S. Uncertainty and sensitivity analysis techniques as tools for the quality assessment of composite indicators. *Journal of the Royal Statistical Society: Series A*, **168**(2), 307–323 (2005)
- [25] ASGHARI, H., TOPOL, H., MARKERT, B., and MERODIO, J. Application of sensitivity analysis in extension, inflation, and torsion of residually stressed circular cylindrical tubes. *Probabilistic Engineering Mechanics*, **73**, 103469 (2023)
- [26] BECKER, W., OAKLEY, J. E., SURACE, C., GILI, P., ROWSON, J., and WORDEN, K. Bayesian sensitivity analysis of a nonlinear finite element model. *Mechanical Systems and Signal Processing*, **32**, 18–31 (2012)
- [27] NARASIMHA, K. V., KUMAR, R. K., and BOHARA, P. C. A sensitivity analysis of design attributes and operating conditions on tyre operating temperatures and rolling resistance using finite element analysis. *Proceedings of the Institution of Mechanical Engineers Part D: Journal of Automob*, **220**(5), 501–517 (2006)
- [28] SCHAFER, F., STURDY, J., MESEK, M., SINEK, A., BIALECKI, R., OSTROWSKI, Z., MELKA, B., NOWAK, M., and HELLEVIK, L. R. Uncertainty quantification and sensitivity analysis during the development and validation of numerical artery models. *ACM Transactions on Modeling and Computer Simulation*, **32**, 256–262 (2022)
- [29] FREY, H. C. and PATIL, S. R. Identification and review of sensitivity analysis methods. *Risk Analysis*, **22**(3), 553–578 (2002)
- [30] ASGHARI, H., TOPOL, H., MARKERT, B., and MERODIO, J. Application of the extended Fourier amplitude sensitivity testing (FAST) method to inflated, axial stretched, and residually stressed cylinders. *Applied Mathematics and Mechanics (English Edition)*, **44**(12), 2139–2162 (2023) <https://doi.org/10.1007/s10483-023-3060-6>
- [31] COWIN, S. C., GAILANI, G., and BENALLA, M. Hierarchical poroelasticity: movement of interstitial fluid between porosity levels in bones. *Philosophical Transactions of the Royal Society A: Mathematical, Physical and Engineering Sciences*, **367**(1902), 3401–3444 (2009)
- [32] PERRIN, E., BOU-SAID, B., and MASSI, F. Numerical modeling of bone as a multiscale poroelastic material by the homogenization technique. *Journal of the Mechanical Behavior of Biomedical Materials*, **91**, 373–382 (2019)

- 
- [33] COWIN, S. C. and CARDOSO, L. Blood and interstitial flow in the hierarchical pore space architecture of bone tissue. *Journal of Biomechanics*, **48**(5), 842–854 (2015)
- [34] SÁNCHEZ, M. T., PÉREZ, M. Á., and GARCÍA-AZNAR, J. M. The role of fluid flow on bone mechanobiology: mathematical modeling and simulation. *Computational Geosciences*, **25**, 823–830 (2021)
- [35] SOLEIMANI, K., GHASEMLOONIA, A., and SUDAK, L. J. Interstitial fluid transport in cortical bone porosities: effects of blood pressure and mass exchange using porous media theory. *Mechanics of Materials*, **193**, 104981 (2024)
- [36] GHIASI, M. S., CHEN, J., VAZIRI, A., RODRIGUEZ, E. K., and NAZARIAN, A. Bone fracture healing in mechanobiological modeling: a review of principles and methods. *Bone Reports*, **6**, 87–100 (2017)
- [37] LIU, C., CARRERA, R., FLAMINI, V., KENNY, L., CABAHUG-ZUCKERMAN, P., GEORGE, B. M., HUNTER, D., LIU, B., SINGH, G., and LEUCHT, P. Effects of mechanical loading on cortical defect repair using a novel mechanobiological model of bone healing. *Bone*, **108**, 145–155 (2018)
- [38] SALTELLI, A., TARANTOLA, S., and CAMPOLONGO, F. Sensitivity analysis as an ingredient of modeling. *Statistical Science*, **15**, 377–395 (2000)
- [39] EFRON, B. and STEIN, C. The jackknife estimate of variance. *Annals of Statistics*, **9**, 586–596 (1981)
- [40] SALTELLI, A. Making best use of model evaluations to compute sensitivity indices. *Computer Physics Communications*, **145**(2), 280–297 (2002)
- [41] ARCHER, G. E. B., SALTELLI, A., and SOBOL, I. M. Sensitivity measures, anova-like techniques, and the use of bootstrap. *Journal of Statistical Computation and Simulation*, **58**(2), 99–120 (1997)
- [42] SOBOL, I. M. Sensitivity analysis for non-linear mathematical models. *Mathematical Modeling and Computational Experiment*, **1**, 407–414 (1993)
- [43] JANON, A., KLEIN, T., LAGNOUX, A., NODET, M., and PRIEUR, C. Asymptotic normality and efficiency of two Sobol index estimators. *ESAIM-Probability and Statistics*, **18**, 342–364 (2014)
- [44] IOOSS, B., VAN, D. F., and DEVICTOR, N. Response surfaces and sensitivity analyses for an environmental model of dose calculations. *Reliability Engineering and System Safety*, **91**(10-11), 1241–1251 (2006)
- [45] SALTELLI, A., ANNONI, P., AZZINI, I., CAMPOLONGO, F., RATTO, M., and TARANTOLA, S. Variance-based sensitivity analysis of model output: design and estimator for the total sensitivity index. *Computer Physics Communications*, **181**(2), 259–270 (2010)
- [46] JANSEN, M. J. W. Analysis of variance designs for model output. *Computer Physics Communications*, **117**(1-2), 35–43 (1999)
- [47] PUY, A., PIANO, S. L., SALTELLI, A., and LEVIN, S. A. Sensobol: an “R” package to compute variance-based sensitivity indices. *Journal of Statistical Software*, **102**, 1–37 (2021)
- [48] LIU, R. and OWEN, A. B. Estimating mean dimensionality of analysis of variance decompositions. *Journal of the American Statistical Association*, **101**(474), 712–721 (2006)
- [49] JOHNSON, N. L., KOTZ, S. I., and BALAKRISHNAN, N. *Beta Distributions*, John Wiley and Sons, New York, 221–235 (1994)
- [50] DEGHANI, H., PENTA, R., and MERODIO, J. The role of porosity and solid matrix compressibility on the mechanical behavior of poroelastic tissues. *Materials Research Express*, **6**(3), 035404 (2018)
- [51] BURRIDGE, R. and KELLER, J. B. Poroelasticity equations derived from microstructure. *The Journal of the Acoustical Society of America*, **70**(4), 1140–1146 (1981)
- [52] LÉVY, T. Propagation of waves in a fluid-saturated porous elastic solid. *International Journal of Engineering Science*, **17**(9), 1005–1014 (1979)
- [53] PENTA, R., MILLER, L., GRILLO, A., RAMÍREZ-TORRES, A., MASCHERONI, P., and RODRÍGUEZ-RAMOS, R. Porosity and diffusion in biological tissues: recent advances and further perspectives. *Constitutive Modelling of Solid Continua*, Springer, Berlin, 311–356 (2020)

- [54] MILLER, L. and PENTA, R. Effective balance equations for poroelastic composites. *Continuum Mechanics and Thermodynamics*, **32**(6), 1533–1557 (2020)
- [55] MILLER, L. and PENTA, R. Double poroelasticity derived from the microstructure. *Acta Mechanica*, **232**, 3801–3823 (2021)
- [56] MILLER, L. and PENTA, R. Investigating the effects of microstructural changes induced by myocardial infarction on the elastic parameters of the heart. *Biomechanics and Modelling in Mechanobiology*, **22**(3), 1019–1033 (2023)
- [57] MILLER, L. and PENTA, R. Micromechanical analysis of the effective stiffness of poroelastic composites. *European Journal of Mechanics/A Solids*, **98**, 104875 (2023)
- [58] RODRIGUEZ, J. and MERODIO, J. A new derivation of the bifurcation conditions of inflated cylindrical membranes of elastic material under axial loading: application to aneurysm formation. *Mechanics Research Communications*, **38**, 203–210 (2010)
- [59] TOPOL, H., AL-CHLAIHAWI, M. J., DEMIRKOPARAN, H., and MERODIO, J. Bulging initiation and propagation in fiber-reinforced swellable mooney-rivlin membranes. *Journal of Engineering Mathematics*, **128**, 1–15 (2021)
- [60] TOPOL, H., AL-CHLAIHAWI, M. J., DEMIRKOPARAN, H., and MERODIO, J. Bifurcation of fiber-reinforced cylindrical membranes under extension, inflation, and swelling. *Applied Computational Mechanics*, **9**, 113–128 (2023)
- [61] SEDDIGHI, Y. and HAN, H. C. Buckling of arteries with noncircular cross sections: theory and finite element simulations. *Frontiers of Physics*, **12**, 712636 (2021)
- [62] FU, Y. B., LIU, J. L., and FRANCISCO, G. S. Localized bulging in an inflated cylindrical tube of arbitrary thickness — the effect of bending stiffness. *Journal of the Mechanics and Physics of Solids*, **90**, 45–60 (2016)
- [63] JHA, N. K., MORADALIZADEH, S., REINOSO, J., TOPOL, H., and MERODIO, J. On the helical buckling of anisotropic tubes with application to arteries. *Mechanics Research Communications*, **128**, 104067 (2023)
- [64] AMBROSI, D., BEN-AMAR, M., CYRON, C. J., DESIMONE, A., GORIELY, A., HUMPHREY, J. D., and KUHL, E. Growth and remodeling of living tissues: perspectives, challenges, and opportunities. *Journal of the Royal Society Interface*, **16**, 20190233 (2019)
- [65] TOPOL, H., DEMIRKOPARAN, H., and PENCE, T. J. On collagen fiber morphoelasticity and homeostatic remodeling tone. *Journal of the Mechanical Behavior of Biomedical Materials*, **113**, 104154 (2021)
- [66] TOPOL, H., DEMIRKOPARAN, H., and PENCE, T. J. Fibrillar collagen: a review of the mechanical modeling of strain-mediated enzymatic turnover. *Applied Mechanics Reviews*, **73**, 050802 (2021)
- [67] SAINI, K., CHO, S., DOOLING, L. J., and DISCHER, D. E. Tension in fibrils suppresses their enzymatic degradation—a molecular mechanism for ‘use it or lose it’. *Matrix Biology*, **85–86**, 34–46 (2020)

## Appendix A

Here, we fully expand the pressure equation (56) for the first 5 calculated  $x_n$  given in Eq. (77). This leaves the pressure as an expression that is now in terms of  $\mu$ ,  $\nu$ ,  $\alpha$ ,  $M$ ,  $P_0$ ,  $R^*$ , and  $t^*$ , i.e.,

$$\begin{aligned}
 p = & (2\alpha P_0(8.7002)^{(3/2)}(1-2\nu)(2\mu(1-\nu)(J_0(R^*\sqrt{8.7002}) - MJ_0(\sqrt{8.7002})) \\
 & - \alpha^2 M(1-2\nu)(J_0(R^*\sqrt{8.7002}) - MJ_0(\sqrt{8.7002})))e^{-8.7002t^*}) \\
 & /((2(1-\nu)\mu^2 - \alpha^2 M\mu(1-2\nu))(J_0(\sqrt{8.7002})\sqrt{8.7002} - 8.7002J_1(\sqrt{8.7002})) \\
 & - 2\alpha^2 M\mu(1-2\nu)^2(J_0(\sqrt{8.7002})\sqrt{8.7002} - J_1(\sqrt{8.7002}))) \\
 & + (2\alpha P_0(34.119)^{(3/2)}(1-2\nu)(2\mu(1-\nu)(J_0(R^*\sqrt{34.119}) - MJ_0(\sqrt{34.119})) \\
 & - \alpha^2 M(1-2\nu)(J_0(R^*\sqrt{34.119}) - MJ_0(\sqrt{34.119})))e^{-34.119t^*})
 \end{aligned}$$

$$\begin{aligned}
& /((2(1-\nu)\mu^2 - \alpha^2 M\mu(1-2\nu))(J_0(\sqrt{34.119})\sqrt{34.119} - 34.119J_1(\sqrt{34.119})) \\
& - 2\alpha^2 M\mu(1-2\nu)^2(J_0(\sqrt{34.119})\sqrt{34.119} - J_1(\sqrt{34.119}))) \\
& + (2\alpha P_0(78.726)^{(3/2)}(1-2\nu)(2\mu(1-\nu)(J_0(R^*\sqrt{78.726}) - MJ_0(\sqrt{78.726})) \\
& - \alpha^2 M(1-2\nu)(J_0(R^*\sqrt{78.726}) - MJ_0(\sqrt{78.726})))e^{-78.726t^*}) \\
& /((2(1-\nu)\mu^2 - \alpha^2 M\mu(1-2\nu))(J_0(\sqrt{78.726})\sqrt{78.726} - 78.726J_1(\sqrt{78.726})) \\
& - 2\alpha^2 M\mu(1-2\nu)^2(J_0(\sqrt{78.726})\sqrt{78.726} - J_1(\sqrt{78.726}))) \\
& + (2\alpha P_0(142.95)^{(3/2)}(1-2\nu)(2\mu(1-\nu)(J_0(R^*\sqrt{142.95}) - MJ_0(\sqrt{142.95})) \\
& - \alpha^2 M(1-2\nu)(J_0(R^*\sqrt{142.95}) - MJ_0(\sqrt{142.95})))e^{-142.95t^*}) \\
& /((2(1-\nu)\mu^2 - \alpha^2 M\mu(1-2\nu))(J_0(\sqrt{142.95})\sqrt{142.95} - 142.95J_1(\sqrt{142.95})) \\
& - 2\alpha^2 M\mu(1-2\nu)^2(J_0(\sqrt{142.95})\sqrt{142.95} - J_1(\sqrt{142.95}))) \\
& + (2\alpha P_0(226.88)^{(3/2)}(1-2\nu)(2\mu(1-\nu)(J_0(R^*\sqrt{226.88}) - MJ_0(\sqrt{226.88})) \\
& - \alpha^2 M(1-2\nu)(J_0(R^*\sqrt{226.88}) - MJ_0(\sqrt{226.88})))e^{-226.88t^*}) \\
& /((2(1-\nu)\mu^2 - \alpha^2 M\mu(1-2\nu))(J_0(\sqrt{226.88})\sqrt{226.88} - 226.88J_1(\sqrt{226.88})) \\
& - 2\alpha^2 M\mu(1-2\nu)^2(J_0(\sqrt{226.88})\sqrt{226.88} - J_1(\sqrt{226.88}))).
\end{aligned}$$

We note that the Bessel functions  $J_0$  and  $J_1$  can easily be evaluated in MATLAB to produce a number, so many more of these terms can be simplified. Therefore, we rewrite as

$$\begin{aligned}
p = & (2\alpha P_0(8.7002)^{(3/2)}(1-2\nu)(2\mu(1-\nu)(J_0(R^*\sqrt{8.7002}) + 0.2425M) \\
& - \alpha^2 M(1-2\nu)(J_0(R^*\sqrt{8.7002}) + 0.2425M))e^{-8.7002t^*}) \\
& /((2(1-\nu)\mu^2 - \alpha^2 M\mu(1-2\nu))(-0.2425\sqrt{8.7002} - 8.7002(0.3576)) \\
& - 2\alpha^2 M\mu(1-2\nu)^2(-0.2425\sqrt{8.7002} - 0.3576)) \\
& + (2\alpha P_0(34.119)^{(3/2)}(1-2\nu)(2\mu(1-\nu)(J_0(R^*\sqrt{34.119}) - 0.1044M) \\
& - \alpha^2 M(1-2\nu)(J_0(R^*\sqrt{34.119}) - 0.1044M))e^{-34.119t^*}) \\
& /((2(1-\nu)\mu^2 - \alpha^2 M\mu(1-2\nu))(0.1044\sqrt{34.119} + 34.119(0.3048)) \\
& - 2\alpha^2 M\mu(1-2\nu)^2(0.1044\sqrt{34.119} + 0.3048)) \\
& + (2\alpha P_0(78.726)^{(3/2)}(1-2\nu)(2\mu(1-\nu)(J_0(R^*\sqrt{78.726}) + 0.0583M) \\
& - \alpha^2 M(1-2\nu)(J_0(R^*\sqrt{78.726}) + 0.0583M))e^{-78.726t^*}) \\
& /((2(1-\nu)\mu^2 - \alpha^2 M\mu(1-2\nu))(-0.0583\sqrt{78.726} - 78.726(0.2584)) \\
& - 2\alpha^2 M\mu(1-2\nu)^2(-0.0583\sqrt{78.726} - 0.2584)) \\
& + (2\alpha P_0(142.95)^{(3/2)}(1-2\nu)(2\mu(1-\nu)(J_0(R^*\sqrt{142.95}) - 0.0378M) \\
& - \alpha^2 M(1-2\nu)(J_0(R^*\sqrt{142.95}) - 0.0378M))e^{-142.95t^*}) \\
& /((2(1-\nu)\mu^2 - \alpha^2 M\mu(1-2\nu))(0.0378\sqrt{142.95} + 142.95(0.2261)) \\
& - 2\alpha^2 M\mu(1-2\nu)^2(0.0378\sqrt{142.95} + 0.2261)) \\
& + (2\alpha P_0(226.88)^{(3/2)}(1-2\nu)(2\mu(1-\nu)(J_0(R^*\sqrt{226.88}) + 0.0269M) \\
& - \alpha^2 M(1-2\nu)(J_0(R^*\sqrt{226.88}) + 0.0269M))e^{-226.88t^*}) \\
& /((2(1-\nu)\mu^2 - \alpha^2 M\mu(1-2\nu))(-0.0269\sqrt{226.88} - 226.88(0.2029)) \\
& - 2\alpha^2 M\mu(1-2\nu)^2(-0.0269\sqrt{226.88} - 0.2029)). \tag{A1}
\end{aligned}$$

This is the fully expanded expression on which the sensitivity analysis in Sections 3 and 4 is performed.